Prompt and Thermally Activated Delayed Fluorescence of Quinazoline-Based Derivatives: a Joint Experimental and Theoretical Study

Maxime Hodée, Tatiana Moshkina, Julien Massue, Arnaud Fihey, Thierry Roisnel, Claudine Katan, Emiliya Nosova, Sylvain Achelle

▶ **To cite this version:**

Maxime Hodée, Tatiana Moshkina, Julien Massue, Arnaud Fihey, Thierry Roisnel, et al.. Prompt and Thermally Activated Delayed Fluorescence of Quinazoline-Based Derivatives: a Joint Experimental and Theoretical Study. ChemPhotoChem, In press, 10.1002/cptc.202400259 . hal-04761690

HAL Id: hal-04761690
https://hal.science/hal-04761690v1

Submitted on 21 Dec 2024

HAL is a multi-disciplinary open access archive for the deposit and dissemination of scientific research documents, whether they are published or not. The documents may come from teaching and research institutions in France or abroad, or from public or private research centers.

L'archive ouverte pluridisciplinaire **HAL**, est destinée au dépôt et à la diffusion de documents scientifiques de niveau recherche, publiés ou non, émanant des établissements d'enseignement et de recherche français ou étrangers, des laboratoires publics ou privés.

Distributed under a Creative Commons Attribution - NonCommercial 4.0 International License

Check for updates

ChemPhotoChem

Research Article
doi.org/10.1002/cptc.202400259

Chemistry Europe
European Chemical Societies Publishing

www.chemphotochem.org

Prompt and Thermally Activated Delayed Fluorescence of Quinazoline-Based Derivatives: A Joint Experimental and Theoretical Study

Maxime Hodée[+],[a] Tatiana N. Moshkina[+],[a, b] Julien Massue,*[c] Arnaud Fihey,*[a] Thierry Roisnel,[a] Claudine Katan,[a] Emiliya Nosova,[b] and Sylvain Achelle*[a]

During the last decade, thermally activated delayed fluorescence has been the topic of intense research due to its great potential for highly efficient all organic light emitting devices. While the quinazoline heterocycle has been used for its electron withdrawing ability in various push-pull dyes, quinazoline derivatives have been rarely considered for TADF emitters. Here we design and synthesize a new series of dyes with phenyl- or methoxy-substituted quinazoline rings combined with 9,9-dimethylacridan, phenoxazine or phenothiazine and either 1,4-phenylene or 2,5-thienylene as linker. Combining optical spectroscopy and theoretical investigations, we demonstrate that delayed fluorescence is observed in the solid state for the phenyl-substituted quinazoline derivatives for which both quasi-equatorial and quasi-axial conformations are predicted to coexist. Calculations further suggest that the reversed intersystem crossing is likely to involve the second triplet state that shows small energy splitting with the first singlet state. These results prompt further investigations of phenyl-substituted quinazoline based dyes for TADF.

Introduction

Thermally activated delayed fluorescence (TADF) is a photophysical process consisting in the involvement of both triplet and singlet states in the emission process, highly advantageous for the engineering of organic light emitting diode (OLED) devices, in which a 1:3 singlet/triplet distribution ratio is obtained after electroexcitation.[1–4] TADF first relies in harvesting of triplet states, followed by a back-transfer through a process called reverse Intersystem Crossing (rISC), upconverting them into singlet states from which fluorescence can take place (Figure 1(a)).[5,6] This phenomenon, which is thermally activated, is mainly driven by two parameters: the spin-orbit coupling (SOC) between the singlet and triplet states of interest, which is evaluated through the spin-orbit coupling matrix element (SOCME) value, and the energy difference between both electronic states, noted ΔE_{ST}, typically required to lie below 0.2 eV for rISC to be effective.[7–10] TADF molecules are commonly based on donor-acceptor (push-pull) structures, in order to favor the presence of a charge transfer (CT) process between the electron-donating (EDG) and -withdrawing (EWG) groups.[5,11] This CT behavior triggers a strong spatial separation of HOMO and LUMO orbitals, which is achieved by the nearly orthogonal alignment of EDG/EWG. In many examples, this configuration leads to a small ΔE_{ST},[4] facilitating the rISC process if there is sufficient thermal energy at room temperature. Furthermore, if the triplet state in the energetic proximity of the CT excited singlet state is of a locally excited (LE) nature, the rISC rate is enhanced, following the well-established "El-Sayed" rule,[12] which states that a change in spin multiplicity must be

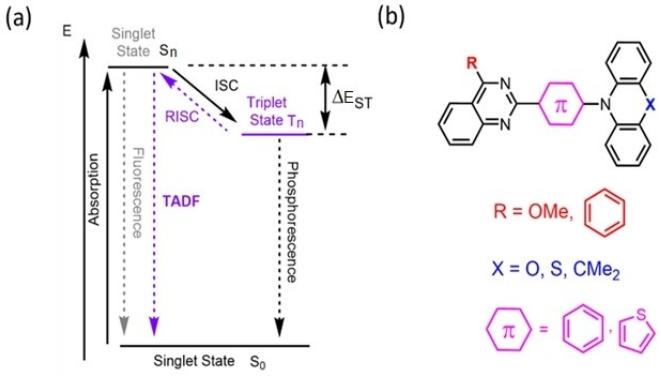

Figure 1. (a) Schematic representation of the TADF process and (b) Structures of the quinazoline-based studied herein.

[a] M. Hodée,[+] T. N. Moshkina,[+] A. Fihey, T. Roisnel, C. Katan, S. Achelle
Univ Rennes, ENSCR, CNRS, ISCR (Institut des Sciences Chimiques de Rennes)-UMR 6226, F-35000 Rennes, France
E-mail: sylvain.achelle@univ-rennes1.fr
arnaud.fihey@univ-rennes1.fr

[b] T. N. Moshkina,[+] E. Nosova
Department of Organic and Biomolecular Chemistry, Ural Federal University, 19 Mira Str., Yekaterinburg 620002, Russian Federation

[c] J. Massue
Institut de Chimie et Procédés pour l'Energie, l'Environnement et la Santé (ICPEES), UMR CNRS 7515, Equipe Chimie Organique pour la Biologie, les Matériaux et l'Optique (COMBO), 25 Rue Becquerel, 67087, Cedex 02 Strasbourg, France
E-mail: massue@unistra.fr

[+] These authors share first authorship.

Supporting information for this article is available on the WWW under https://doi.org/10.1002/cptc.202400259

© 2024 The Author(s). ChemPhotoChem published by Wiley-VCH GmbH. This is an open access article under the terms of the Creative Commons Attribution Non-Commercial License, which permits use, distribution and reproduction in any medium, provided the original work is properly cited and is not used for commercial purposes.

© 2024 The Author(s). ChemPhotoChem published by Wiley-VCH GmbH

23670932, 0, Downloaded from https://chemistry-europe.onlinelibrary.wiley.com/doi/10.1002/cptc.202400259 by Université De Rennes, Wiley Online Library on [13/11/2024]. See the Terms and Conditions (https://onlinelibrary.wiley.com/terms-and-conditions) on Wiley Online Library for rules of use; OA articles are governed by the applicable Creative Commons License

accompanied by a change in angular momentum of the system, increasing the SOCME value.[7–9,13–15] Both a strong SOC and a low ΔE_{ST} contribute to the rISC, where the nature of the singlet and triplet states is key to the presence of TADF. The pronounced CT nature of the first singlet state S_1 can potentially result in fluorescence quenching, as the strong decoupling between EDG and EWG can lead to minimal orbital overlap, thereby hindering efficient emission. In order to mitigate the CT nature of S_1, it appears imperative to design orthogonal push-pull structures, which have the flexibility to deviate from a strictly 90° arrangement, prone to non-radiative deactivation. This synthetic strategy may be combined with that targeting coexistence of several conformers, especially in the solid state. In this context, several systems exhibiting excited states with an electronic configuration in between LE and CT characters, referred to as hybridized local charge transfer (HLCT) states circumventing the orthogonal structure limitations, have been recently reported.[16–20] This HLCT character has been demonstrated to be beneficial to rISC process since it satisfies the El-Sayed rule while at the same time enabling sufficiently small ΔE_{ST}.[21]

The quinazoline (or benzopyrimidine) heterocycle is a bicyclic aromatic fragment exhibiting a π-deficient character, which has been involved in various push-pull derivatives as EWG, exhibiting modular CT-controlled fluorescence emission.[22–28] However, to the best of our knowledge, only a few quinazoline-based TADF systems have been described so far.[29–34] Using these emitters, third generation OLED devices with external quantum efficiency up to 28% have been reported.[31]

In this contribution, we designed a series of chromophores, with potential for HLCT and/or dual conformation, involving phenyl- or methoxy-substituted quinazoline rings, as EWG and sterically hindered EDG such as 9,9-dimethylacridan (DMAC), phenoxazine (PXZ) or phenothiazine (PTZ) (Figure 1b). The nature of the π-conjugated bridge between donor and acceptor parts of the dyad was also modified, *ie* either a 1,4-phenylene or a 2,5-thienylene tether was introduced. Based on a combined experimental and theoretical approach, the emission properties of these molecules were rationalized and their efficiency as TADF emitters was investigated and discussed.

Results and Discussion

Synthesis

The synthetic approach to the target molecules is depicted in Schemes 1 and 2. 4-Phenylquinazolines **1** and **2** were prepared according to literature protocol from 2-aminobenzophenone and corresponding aldehydes.[35] 4-Methoxyquinazoline **3** was synthesized by aromatic nucleophilic substitution following a reported procedure[36] starting from 4-chloroquinazoline.[37] All compounds were obtained from intermediates **1**–**3** by Buchwald-Hartwig cross-coupling reaction, with 9,9-dimethyl-9,10-dihydroacridine, phenoxazine or phenothiazine as coupling partners.[38,39] It should be noted that in case of thiophene intermediate **2**, a stronger base (*t*BuONa) and a different Pd catalyst (Pd_2dba_3) are required.[40,41] All compounds were

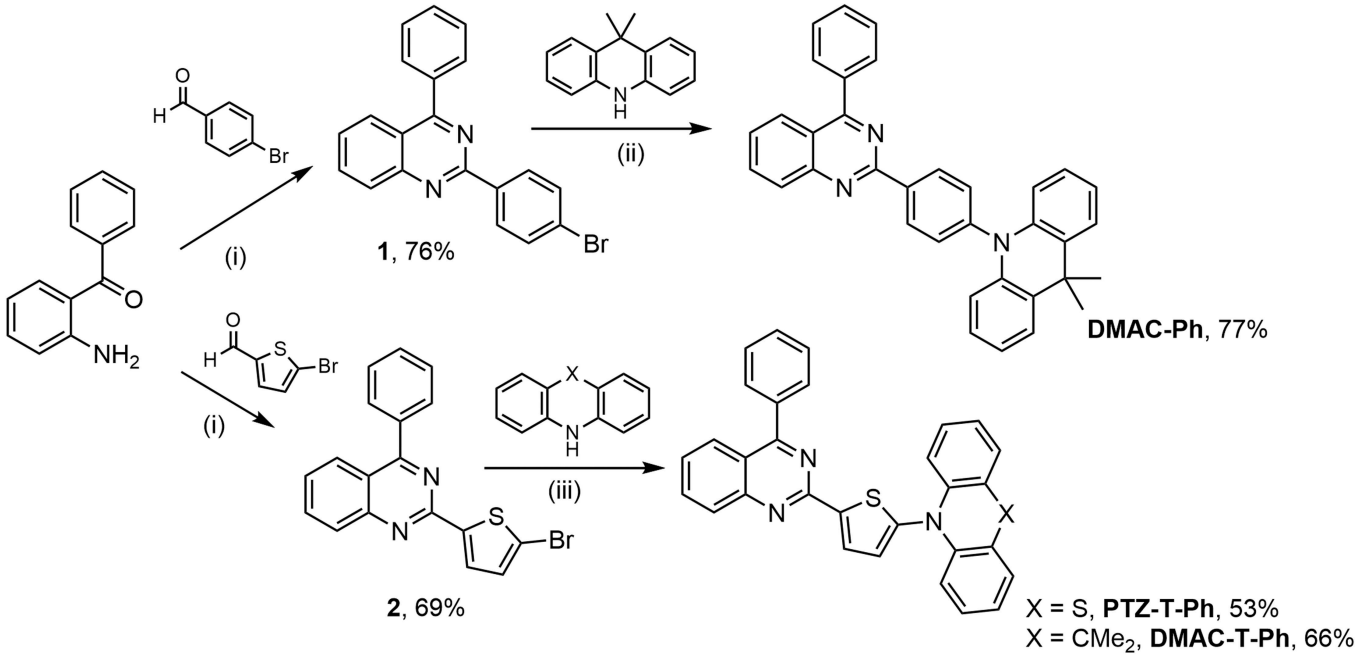

(i) $AcONH_4$, I_2, EtOH, r.t., 19 or 24 h, (ii) $Pd(OAc)_2$, $P(tBu)_3HBF_4$, K_2CO_3, toluene, N_2, Δ, 3 days, (iii) Pd_2dba_3, $P(tBu)_3HBF_4$, *t*BuONa, toluene, N_2, Δ, 3 days.

Scheme 1. Synthesis of 4-phenylquinazoline derivatives **DMAC-Ph**, **PTZ-T-Ph** and **DMAC-T-Ph**.

© 2024 The Author(s). ChemPhotoChem published by Wiley-VCH GmbH

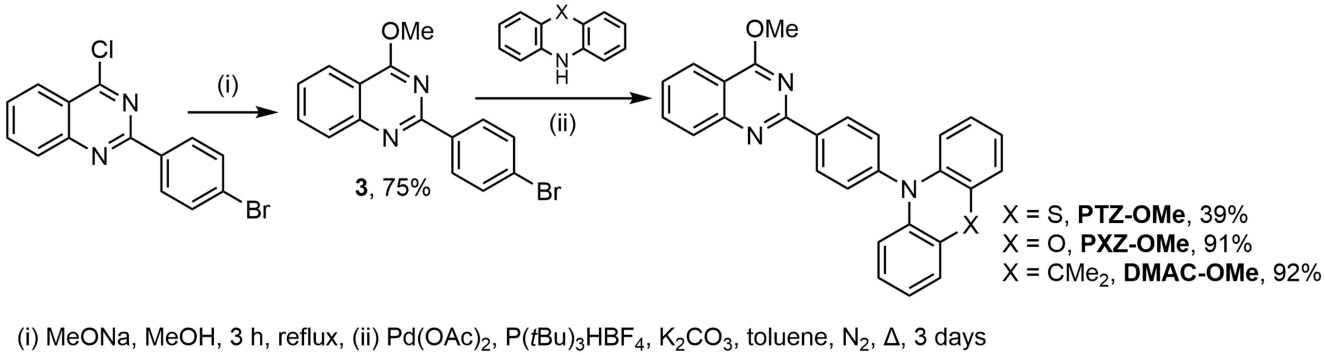

(i) MeONa, MeOH, 3 h, reflux, (ii) $Pd(OAc)_2$, $P(tBu)_3HBF_4$, K_2CO_3, toluene, N_2, Δ, 3 days

Scheme 2. Synthesis of 4-methoxyquinazoline derivatives, **PTZ-OMe**, **PXZ-OMe** and **DMAC-OMe**.

characterized by ^1H and ^{13}C NMR as well as HR-MS to confirm their molecular structure (see experimental section).

X-ray Analysis and DFT Ground State Geometry

Single crystals of quinazoline **PTZ-OMe** were grown by slow evaporation of chloroform at room temperature and analyzed by X-ray crystallography (CCDC 2339313). The measured crystal, a colorless prism, confirmed the proposed molecular structure. Crystal structure has been described in triclinic symmetry and P $\bar{1}$ (I.T.#2) centric space group. Cell parameters have been refined as follows: a = 7.9906(13), b = 11.9768(16), c = 12.6868(17) Å, α = 62.514(4), β = 86.926(5), γ = 77.004(5)°, V = 1047.7(3) Å^3. The dihedral angle between the quinazoline and the phenyl fragment in C2 position is around 6° in accordance with known structure of 2-phenylquinazoline derivatives (Figure 2).[42]

Various authors have described the existence of two different conformations for acridan derivatives as well as phenoxazine and phenothiazine analogues, called Quasi-Equatorial (QE), with the donor and acceptor moieties perpendicular to each other, and Quasi-Axial (QA), in which the donor moiety adopts a folded structure bent by about 50° (see angle **Φ** in Table S3 and Figure S41) towards the acceptor-linker plane, both shown schematically in Figure 2.[43–47] In these works, the role of both conformers was highlighted as crucial, largely because it permits dual fluorescence in such compounds, both conformers emitting at different wavelengths. In the work of Li et al. describing phenoxazine substituted quinazoline, the different conformations QE/QA were not considered.[33] In our work, due to the presence of acridan derivatives, the investigation of both conformers is necessary to rationalize fully the experimental emission spectra and the photophysical fingerprint of such conformers. It is also to be noted that in multiple works, rISC is described to occur prevalently in the perpendicular QE conformer.[45,47] Thus, investigation of the delayed fluorescence capacity of both conformations is necessary to assess the whole photochemical picture. The X-ray analyses revealed a QE conformation in the solid state for **PTZ-OMe**, as observed previously for PXZ analogues,[33] with vertical torsion angle between the phenothiazine donor and the phenyl bridge of 86°, as represented in Figure 2.

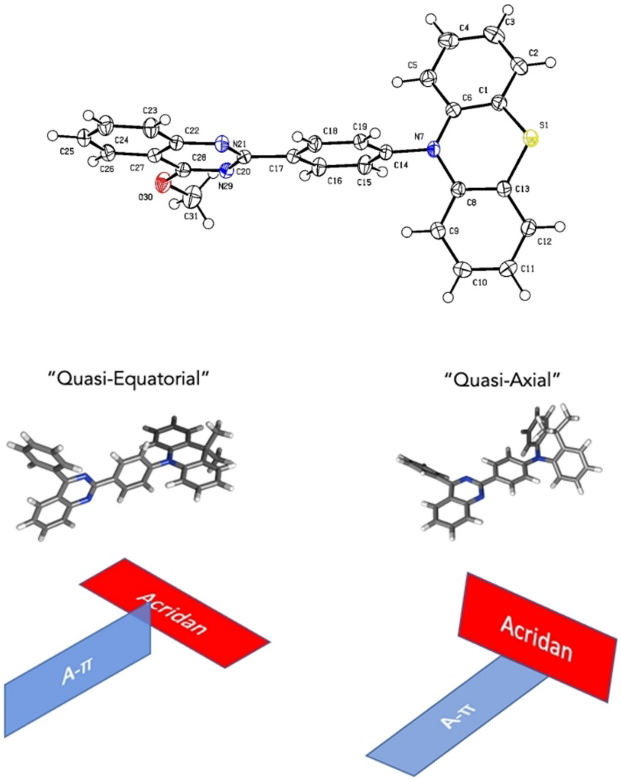

Figure 2. Top: ORTEP drawing of chromophore **PTZ-OMe** obtained at 150 K (R = 0.04). Thermal ellipsoids are shown at the 50% probability level. Bottom: illustration of the Quasi-Equatorial (QE)/Quasi-Axial (QA) conformations exemplified with **DMAC-Ph**, along with a schematic representation of both conformers.

In solution, both QE and QA may coexist; Table 1 presents the calculated Gibbs free energy difference, ΔG, between the QE and QA conformers for the whole series in the ground state. In the cases of **DMAC-Ph**, **DMAC-T-Ph** and **PTZ-T-Ph**, the two conformers are found to be almost equally stable, in slight favor of QE with a ΔG between 0.17 kJ.mol^{-1} (**DMAC-T-Ph**) and 1.28 kJ.mol^{-1} (**DMAC-Ph**), suggesting a possible coexistence at room temperature. No QA minima were obtained for **DMAC-OMe** and **PXZ-OMe**. Noticeably, and unlike the planar DMAC group, the PXZ and PTZ donor moieties of the QE conformers are found to adopt a "butterfly-like" structure in the optimized

© 2024 The Author(s). ChemPhotoChem published by Wiley-VCH GmbH

23670932, 0, Downloaded from https://chemistry-europe.onlinelibrary.wiley.com/doi/10.1002/cptc.202400259 by Université De Rennes, Wiley Online Library on [13/11/2024]. See the Terms and Conditions (https://onlinelibrary.wiley.com/terms-and-conditions) on Wiley Online Library for rules of use; OA articles are governed by the applicable Creative Commons License

Table 1. Gibbs free energy difference, ΔG, between the QE and QA conformers at the ground state, along with the respective Boltzmann population of the most stable one. Values reported are relative to the minimum, which is the QE conformer in all cases.

	ΔG (kj.mol^{-1})	%Population
DMAC-Ph	1.28	63
DMAC-T-Ph	0.17	52
PTZ-T-Ph	0.85	58
PTZ-OMe	2.79	76
DMAC-OMe	No QA minima found	
PXZ-OMe		

ground state, with a torsion angle of about 145–160° (angle γ in Table S3 and Figure S41) around the heteroatom.

Photophysical Studies

The absorption and photoluminescence (PL) spectra of all quinazoline dyes in solution (in toluene, *n*-heptane and methyl-THF) and solid PMMA films (as 1% wt) are presented in Figures 3 and 4 and in the SI. Their experimental and computed photophysical data are collected in Tables 2 and 3, S1 and S2.

All the derivatives were characterized by a low-lying absorption band centered between 340 and 400 nm, mostly independent of the solvent polarity, with absorption coefficients in the range 1600–8500 $M^{-1}cm^{-1}$ and additional absorption bands, observed below 300 nm. As far as the low-lying absorption band is concerned, the thienylene linker and the replacement of phenyl substituent by a methoxy one on the quinazoline core induces a blue shift (**DMAC-T-Ph** and **DMAC-OMe** *vs* **DMAC-Ph**). In the 2-methoxyquinazoline series of chromophores, the absorption band is red-shifted in the following order **PTZ-OMe** < **DMAC-OMe** < **PXZ-OMe** as observed with other similar series of chromophores.[38] The excitation energies and oscillator strengths computed in gas phase are reported for both QE and QA conformers in Table 3.

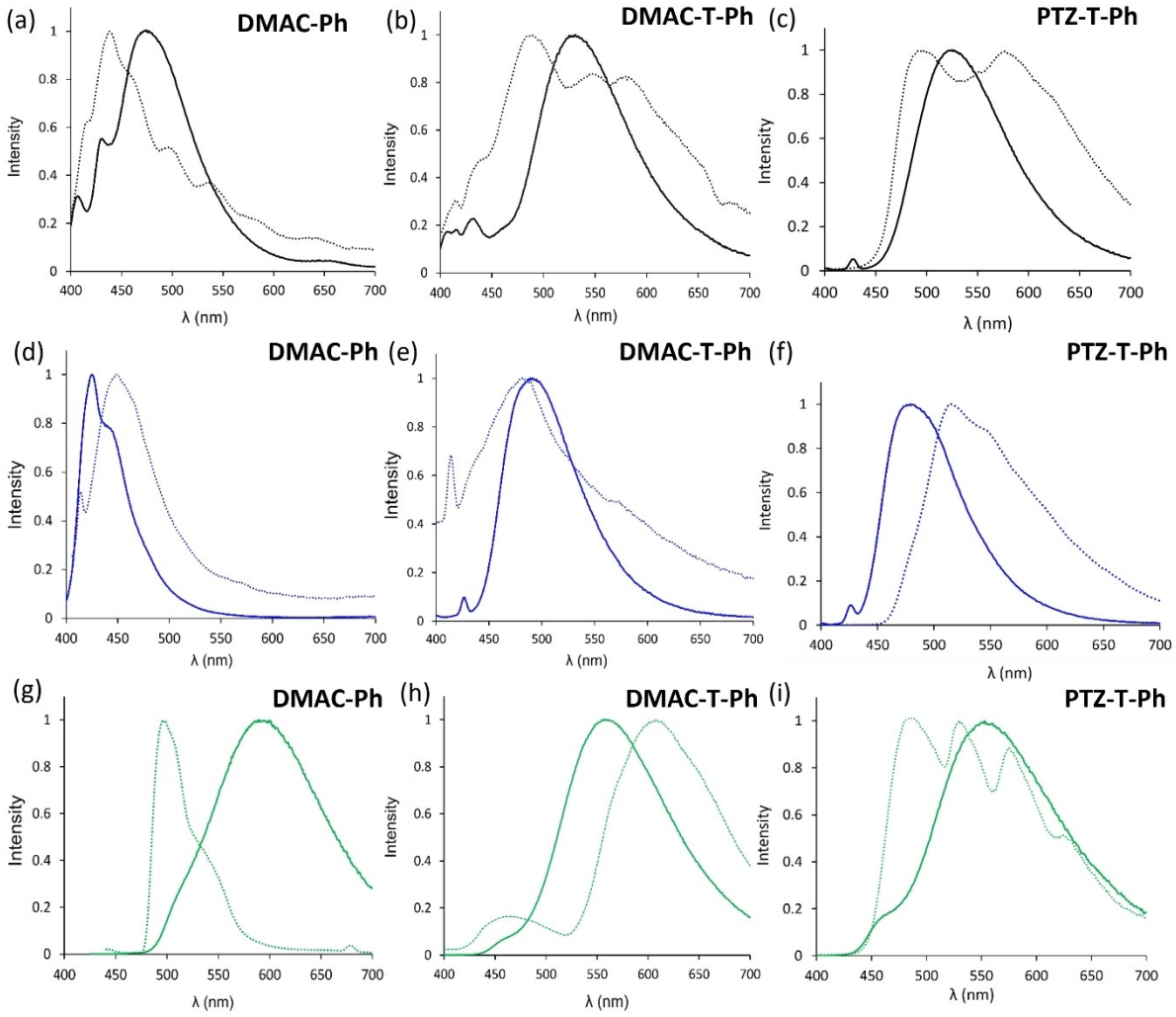

Figure 3. Normalized emission spectra at 25 °C (plain) and 77 K (dotted) of **DMAC-Ph**, **DMAC-T-Ph** and **PTZ-T-Ph** in (a)–(c) toluene, (d)–(f) n-heptane and (g)–(i) Me-THF. Excitation was performed at absorption maximum.

© 2024 The Author(s). ChemPhotoChem published by Wiley-VCH GmbH

23670932, 0, Downloaded from https://chemistry-europe.onlinelibrary.wiley.com/doi/10.1002/cptc.202400259 by Université De Rennes, Wiley Online Library on [13/11/2024]. See the Terms and Conditions (https://onlinelibrary.wiley.com/terms-and-conditions) on Wiley Online Library for rules of use; OA articles are governed by the applicable Creative Commons License

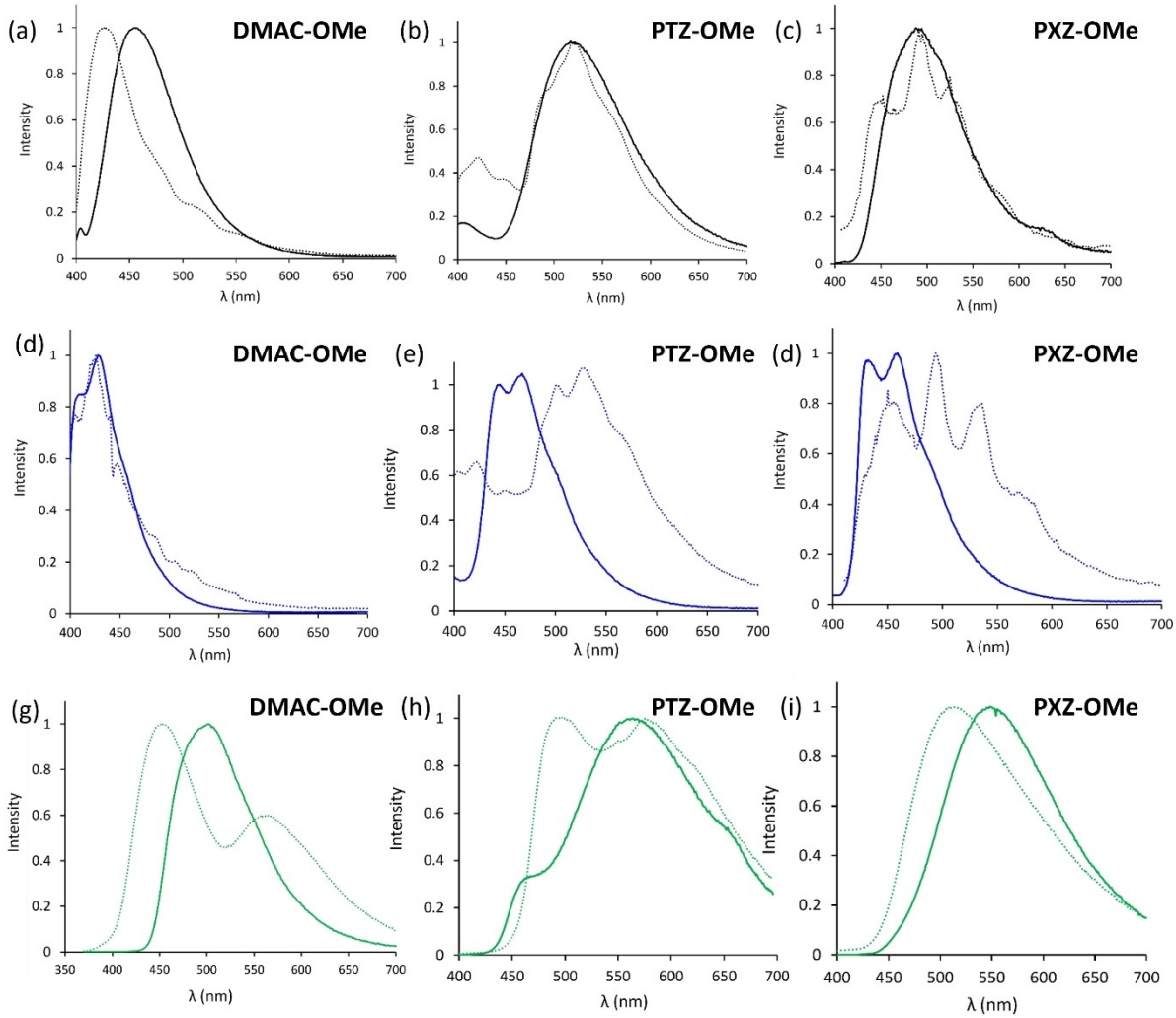

Figure 4. Normalized emission spectra at 25 °C (plain) and 77 K (dotted) of **DMAC-OMe**, **PTZ-OMe** and **PXZ-OMe** in (a)–(c) toluene, (d)–(f) n-heptane and (g)–(i) Me-THF. Excitation was performed at absorption maximum.

For all fluorophores, the QE conformer presents a $S_0 \rightarrow S_1$ transition with low or near-zero oscillator strength. These low-lying transitions lie in between 3.67 eV (338 nm) for **DMAC-Ph** and 3.95 eV (314 nm) for **PTZ-OMe**. The corresponding NTOs (Natural Transition Orbitals)[48] are reported for **DMAC-Ph** in Figure 5 (NTOs for the other molecules are shown in Figures S42–S47) and exhibit a clear CT character from the donor to the quinazoline moiety except for **PTZ**-based chromophores. Notably, for **PTZ-T-Ph** this lowest energy transition is still non-negligibly allowed, ($f = 0.12$), as a result of the LE character of the excitation, as illustrated in Figure S44. A more intense excitation is found higher in energy, between 3.89 eV (**DMAC-T-Ph**) and 4.60 eV (**DMAC-Ph**). Such excitations towards higher excited states show oscillator strengths between 0.13 for **DMAC-T-Ph** and 0.71 for **PTZ-T-Ph** and correspond to a localized π-π^* transition (see Figure 5). For the three phenyl-substituted compounds and **PTZ-OMe**, the excitations in the QA conformers are significantly different, with a lowest energy transition optically allowed and an oscillator strength around 0.4 or higher. For the three phenyl-quinazoline derivatives this is related to a prevalent LE nature of the excitation (illustrated for **DMAC-Ph** in Figure 5 and in the ESI for the others), delocalized over a large part of the π-conjugated structure, whereas for **PTZ-OMe** NTOs reveal a clear HLCT character. The absorption of the QA conformation is thus expected to contribute non-negligibly to the experimental low energy absorption bands.

After photoexcitation in the lowest-energy absorption bands at room temperature (25 °C), all dyes exhibit an intense single emission band in solution in the range 426–491 nm in *n*-heptane, 459–530 nm in toluene and 501–597 nm in Me-THF (Figures 3 and 4). The replacement of the phenyl substituent by a methoxy one on the quinazoline core leads to a blue shift of emission (**DMAC-OMe** *vs* **DMAC-Ph**). Moreover, contrary to what is observed in absorption, the presence of thienylene linker induces a redshift of emission (**DMAC-T-Ph** *vs* **DMAC-Ph**) and in the methoxyquinazoline series, phenothiazine and phenoxazine derivatives **PTZ-OMe** and **PXZ-OMe** exhibit significantly red-shifted emission whatever the matrix with regards to dimethylacridan derivative **DMAC-OMe**. For all chromophores,

© 2024 The Author(s). ChemPhotoChem published by Wiley-VCH GmbH

23670932, 0, Downloaded from https://chemistry-europe.onlinelibrary.wiley.com/doi/10.1002/cptc.202400259 by Université De Rennes, Wiley Online Library on [13/11/2024]. See the Terms and Conditions (https://onlinelibrary.wiley.com/terms-and-conditions) on Wiley Online Library for rules of use; OA articles are governed by the applicable Creative Commons License

Table 2. Photophysical data in solution and in PMMA films for quinazoline-based fluorophores.

Dye	Matrix	λ_{abs} (nm)	$\varepsilon\times10^{-3}$ ($M^{-1}.cm^{-1}$)	λ_{em} (nm)	QY aerated	QY degassed
DMAC-Ph	toluene	385	2.2	477[b] (438)[c]	0.13[d]	0.15[d]
	n-heptane	386	1.8	426[b] (449)[c]	0.21[d]	0.25[d]
	MeTHF	383	4.3	597[b] (499)[c]	0.03[d]	0.04[d]
	PMMA[a]	370	–	457	0.15[e]	–
DMAC-T-Ph	toluene	370	4.0	530[b] (490)[c]	0.35[d]	0.40[d]
	n-heptane	383	1.6	491[b] (482)[c]	0.20[d]	0.27[d]
	MeTHF	361	6.3	562[b] (609)[c]	0.08[d]	0.10[d]
	PMMA[a]	360	–	466	0.17[e]	–
PTZ-T-Ph	toluene	404	4.8	527[b](497/577)[c]	0.06[d]	0.10[d]
	n-heptane	396	5.8	482[b] (516)[c]	0.09[d]	0.15[d]
	MeTHF	367	8.5	555[b](485/530/578)[c]	0.02[d]	0.05[d]
	PMMA[a]	360	–	467	0.12[e]	–
DMAC-OMe	toluene	369	2.0	459[b] (426)[c]	0.15[d]	0.15[d]
	n-heptane	368	2.2	430[b] (425)[c]	0.16[d]	0.18[d]
	MeTHF	370	3.8	501[b] (453)[c]	0.06[d]	0.07[d]
	PMMA[a]	360	–	425	0.08[e]	–
PTZ-OMe	toluene	343	6.8	522[b] (522)[c]	0.03[d]	0.06[d]
	n-heptane	351	2.9	468[b] (528)[c]	0.02[d]	0.07[d]
	MeTHF	364	5.3	561[b] (412)[c]	0.02[d]	0.05[d]
	PMMA[a]	360	–	467	0.10[e]	–
PXZ-OMe	toluene	390	1.7	491[b] (492)[c]	0.24[d]	0.27[d]
	n-heptane	393	4.4	489[b] (495)[c]	0.10[d]	0.12[d]
	MeTHF	386	3.1	550[b] (512)[c]	0.06[d]	0.08[d]
	PMMA[a]	360	–	483	0.15[e]	–

[a] 1 % wt of dyes doped in PMMA films. [b] Emission maximum wavelength at room temperature. [c] Measured at 77 K. [d] Relative quantum yield ($\pm$0.05) determined in solution using Rhodamine 6 G as a reference (λ_{exc} = 488 nm, Φ = 0.88 in ethanol), [e] Absolute quantum yield, calculated with an integrating sphere.

Table 3. Computed absorption and emission properties in gas phase. Energies (wavelengths) of absorption and emission $E_{abs/em}$ ($\lambda_{abs/em}$) in eV (nm) are given, along with the oscillator strengths $f_{abs/em}$. The lowest energy transition as well as the first intense ($f > 0.1$) transition are presented (when they are not the same).

Compound	Conformation	E_{abs} (λ_{abs})	f_{abs}	Transition	E_{em} (λ_{em})	f_{em}
DMAC-Ph	QE	3.67 (338)	0	$S_0\rightarrow S_1$	2.80 (443)	0
		4.60 (269)	0.25	$S_0\rightarrow S_7$		
	QA	3.63 (341)	0.43	$S_0\rightarrow S_1$	3.02 (410)	0.20
DMAC-T-Ph	QE	3.70 (335)	0	$S_0\rightarrow S_1$	2.85 (435)	0.01
		3.89 (319)	0.13	$S_0\rightarrow S_2$		
	QA	3.30 (376)	0.54	$S_0\rightarrow S_1$	2.61 (475)	0.18
PTZ-T-Ph	QE	3.90 (317)	0.12	$S_0\rightarrow S_1$	2.60 (477)	0.06
		4.35 (285)	0.71	$S_0\rightarrow S_6$		
	QA	3.42 (362)	0.39	$S_0\rightarrow S_1$	2.64 (470)	0.17
DMAC-OMe	QE	3.76 (330)	0	$S_0\rightarrow S_1$	3.25 (381)	0.24
		4.60 (269)	0.35	$S_0\rightarrow S_5$		
PTZ-OMe	QE	3.95 (314)	0	$S_0\rightarrow S_1$	2.93 (418)	0
		4.62 (268)	0.62	$S_0\rightarrow S_7$		
	QA	4.10 (302)	0.51	$S_0\rightarrow S_1$	2.64 (470)	0.17
PXZ-OMe	QE	3.78 (328)	0	$S_0\rightarrow S_1$	2.98 (416)	0.21
		4.30 (288)	0.14	$S_0\rightarrow S_3$		

© 2024 The Author(s). ChemPhotoChem published by Wiley-VCH GmbH

23670932, 0, Downloaded from https://chemistry-europe.onlinelibrary.wiley.com/doi/10.1002/cptc.202400259 by Université De Rennes, Wiley Online Library on [13/11/2024]. See the Terms and Conditions (https://onlinelibrary.wiley.com/terms-and-conditions) on Wiley Online Library for rules of use; OA articles are governed by the applicable Creative Commons License

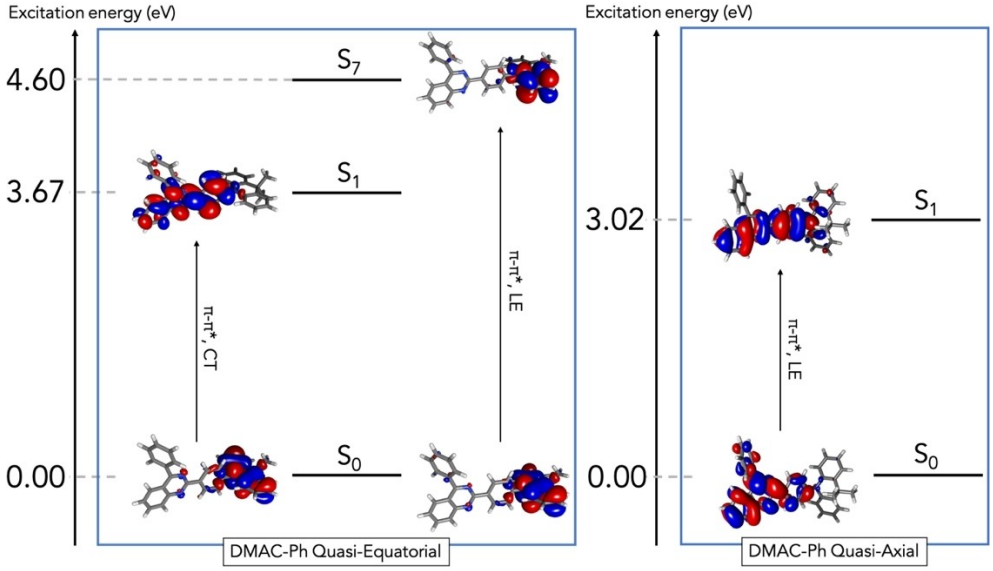

Figure 5. Computed vertical excitation energies and NTOs for the ground state QE and QA geometries of **DMAC-Ph** (isovalue = 0.02 e^-/au^3).

the bathochromic shift of the maximum emission wavelength observed with increasing polarity of the solvent is clearly indicative of an ICT-controlled singlet state. This trend is more marked with the phenyl-quinazoline series, as compared to the methoxy-quinazoline one, consistent with the increase of the electron-withdrawing ability of the former one. To further investigate this ICT process, emission spectra were also recorded at 77 K (Figures 3 and 4). At low temperature, different behaviors are encountered, with either a sole blue-shift of the fluorescence band, consistent with the absence of ICT process or the concomitant appearance of a red-shifted band, often coalesced with fluorescence, tentatively attributed to the presence of a triplet state T_n. The photoluminescence quantum yields (PLQY) of all quinazoline compounds were determined under aerated and degassed conditions at room temperature to investigate the possibility of triplet state harvesting, involved in the radiative pathway (Table 2). PLQY appears to vary in a negligible amount in the absence of oxygen in solution, presumably revealing the absence of accessible triplet states at room temperature. The highest PLQY in degassed toluene is observed for **DMAC-T-Ph** (0.40). The emission spectra of all compounds were also studied in PMMA thin films as doped in 1 % wt (Figures S35 and S36). Similar features as those observed in solution are present in solid, *ie* presence of a single fluorescence band in the range 425–483 nm with a more pronounced structuration.

Quantum chemistry was further used to investigate the impact of the potential coexistence of QE and QA conformers on the emission properties. Noticeably, after relaxation in the first excited state of the QE conformers, the torsion angle between the donor moieties and the phenyl or thiophene linker decreases substantially (see angles Θ and Θ′ in Table S4). In addition, the structure of the phenothiazine and phenoxazine donor groups becomes nearly planar in this S_1 state, (angle γ in Table S4) as already reported by other groups for such donor moieties.[49,50] Table 3 reports the calculated energies and oscillator strengths of the de-excitation from this first singlet excited state to the ground state ($S_1 \rightarrow S_0$). For QE conformers, phenyl-substituted compounds and **PTZ-OMe** show small to near zero oscillator strengths, while in **DMAC-OMe** and **PXZ-OMe** this transition is found more intense (*f* of 0.24 and 0.21) and peaks at higher energies. This difference is rationalized by representing the corresponding NTOs in Figure 6. Notably, for **DMAC-Ph** and **DMAC-T-Ph** the $S_1 \rightarrow S_0$ show a n–π* character, as already reported for other benzoannelated diazines.[51] Even so **PTZ-OMe** has a π–π*/LE character, it corresponds to an inversion symmetry-induced parity-forbidden transition with vanishing oscillator strength. For the three remaining compounds, **PTZ-T-Ph**, **DMAC-OMe** and **PXZ-OMe**, the π–π* transition gains a degree of hybrid character which reduces (increases) the oscillator strength for the former (later). For the QA conformations the de-excitation is found with oscillator strengths of about 0.20, systematically larger than for the QE conformations, and energies ranging between 2.61 eV (**DMAC-T-Ph**) to 3.02 eV (**DMAC-Ph**). The QA conformer of **PTZ-OMe** has a π–π* transition with a clear HLCT character, delocalized over the whole molecular backbone. For the $S_1 \rightarrow S_0$ transition of the other QA conformers, the π–π*/LE character observed for excitation is preserved with a particle in the NTO representation slightly less delocalized, leading to a reduction of oscillator strength compared to the $S_0 \rightarrow S_1$ excitation. If the multiple emission bands seen in the experimental emission spectra (Figures 3 and 4) remain difficult to attribute precisely to theoretical results obtained in gas phase, the presence of both conformers, in varying proportion is expected to contribute to this complex behavior, as hinted by the temperature-dependent observations as well as different behaviors between solution and solid-state PMMA matrix (vide infra).[43,44] It is noteworthy that the computed emission of the QA of **PTZ-OMe** and **DMAC-T-Ph** is red-shifted compared to the QE, in contrast

© 2024 The Author(s). ChemPhotoChem published by Wiley-VCH GmbH

23670932, 0, Downloaded from https://chemistry-europe.onlinelibrary.wiley.com/doi/10.1002/cptc.202400259 by Université De Rennes, Wiley Online Library on [13/11/2024]. See the Terms and Conditions (https://onlinelibrary.wiley.com/terms-and-conditions) on Wiley Online Library for rules of use; OA articles are governed by the applicable Creative Commons License

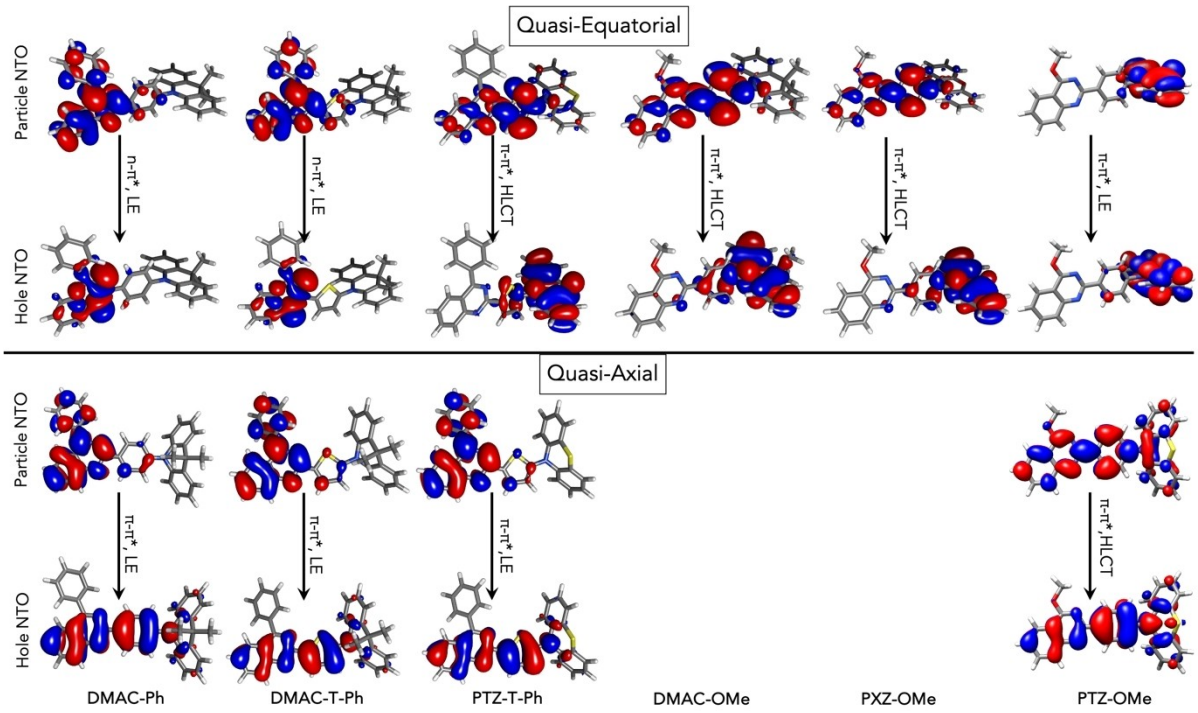

Figure 6. NTOs computed at the geometry of the first singlet state relevant to the de-excitation process from S_1 to S_0 (isovalue of 0.02 e^-/au^3).

to the rest of the series. For the former, the QE emission presents a very localized character, centered on the electron-donating group, while in the QA conformer, the same transition is delocalized over the whole molecular structure. For the latter, **DMAC-T-Ph** is the only compound in this study exhibiting an n–π* emission of the excited QE conformation. These two transitions from the first excited singlet display markedly different behavior from that observed in other systems of the series, leading to the opposite trend in energy shifts.

Delayed Emission

The time-resolved behavior of the six chromophores was investigated in solution and in PMMA thin films (Table 4 and S1–S2). In solution, all dyes were found to decay in the nanosecond regime, consistent with short-lived organic fluorescence. But for the 4-phenylquinazoline derivatives **DMAC-Ph**, **DMAC-T-Ph** and **PTZ-T-Ph** in PMMA films, a long-lived lifetime was recorded, which does coexist with the prompt fluorescence. The recorded delayed lifetimes of 2.3, 1.5 and

Table 4. Time-resolved parameters of quinazoline derivatives in MeTHF solution and PMMA films, along with estimation of the first singlet $E(S_1)$, the triplet E(T) energies as well as ΔE_{ST}.

Dye	Matrix	τ_{PF} (ns)	τ_{DF} (μs)	$\lambda_{em}(S_1)$ (nm)	$\lambda_{em}(T)$ (nm)	$E(S_1)$ (eV)	E(T) (eV)	ΔE_{ST}[a] (eV)
DMAC-Ph	MeTHF	10.2	–	597	650	2.55	2.19	0.36
	PMMA	9.9	2.3	457	525	3.13	2.95	0.18
DMAC-T-Ph	MeTHF	4.5	–	562	590	2.83	2.38	0.45
	PMMA	8.9	1.5	466	558	3.01	2.87	0.14
PTZ-T-Ph	MeTHF	4.0	–	555	473	2.80	2.47	0.33
	PMMA	8.5	1.2	467	572	3.14	2.95	0.19
DMAC-OMe	MeTHF	6.8	–	501	553	2.81	2.57	0.24
	PMMA	14.2	–	425	484	3.35	2.95	0.40
PTZ-OMe	MeTHF	7.3	–	561	580	2.88	2.25	0.63
	PMMA	35.6	–	467	525	3.29	2.64	0.65
PXZ-OMe	MeTHF	8.1	–	550	588	2.84	2.53	0.31
	PMMA	27.4	–	483	512	3.08	2.76	0.32

[a] $\Delta E_{ST} = E(S) - E(T)$. E(S) is the energy determined from the onset of the fluorescence spectrum in MeTHF matrix at 77 K. E(T) was determined from the first peak of the phosphorescence spectrum in MeTHF at 77 K.

© 2024 The Author(s). ChemPhotoChem published by Wiley-VCH GmbH

23670932, 0, Downloaded from https://chemistry-europe.onlinelibrary.wiley.com/doi/10.1002/cptc.202400259 by Université De Rennes, Wiley Online Library on [13/11/2024]. See the Terms and Conditions (https://onlinelibrary.wiley.com/terms-and-conditions) on Wiley Online Library for rules of use; OA articles are governed by the applicable Creative Commons License

23670932, 0, Downloaded from https://chemistry-europe.onlinelibrary.wiley.com/doi/10.1002/cptc.202400259 by Université De Rennes, Wiley Online Library on [13/11/2024]. See the Terms and Conditions (https://onlinelibrary.wiley.com/terms-and-conditions) on Wiley Online Library for rules of use; OA articles are governed by the applicable Creative Commons License

1.2 μs, respectively, can be tentatively ascribed to TADF emission. This motivated further investigations to experimentally estimate the energy difference ΔE_{ST} in Me-THF solution as well as in PMMA thin films (Table 4). The large ΔE_{ST} values (i.e. >0.2 eV) extracted for all compounds in Me-THF solutions are consistent with the observation of short-lived fluorescence and most likely marginal rISC. The same holds for the fluorophores bearing a methoxy-substituted quinazoline ring. On the other hand, the ΔE_{ST} values extracted for **DMAC-Ph**, **DMAC-T-Ph** and **PTZ-T-Ph** in PMMA films are all below 0.2 eV, which is consistent with rISC and TADF at room temperature.

To provide further insights into the nature of the potential triplet states involved in TADF, triplet states were also investigated theoretically in gas phase. Relaxed geometries of the T_1 and T_2 states exhibit similarities to the relaxed S_1 state (see Tables S4–S6 of the ESI). Table 5 reports the computed singlet-triplet energy splitting which is defined as the adiabatic energy difference between the energies of the potential minima for the first excited singlet and the triplet state of interest.[7] The corresponding Spin-Orbit Coupling Matrix Elements (SOCME), obtained at the respective triplet state geometries, are also computed. In all cases, the T_1 state is found below the S_1 state with computed $\Delta E_{S_1T_1}$ values ranging between 0.38 eV and 0.89 eV. The smallest $\Delta E_{S_1T_1}$ values are computed for **PXZ-OMe** and **PTZ-OMe**, yet these two chromophores present the smallest $SOCME_{S_1T_1}$, which is not favorable to rISC. Even though other molecules have significantly larger $SOCME_{S_1T_1}$, between 0.4 cm^{-1} for **DMAC-OMe** and 1.5 cm^{-1} for the QE conformer of **DMAC-Ph**, computed $\Delta E_{S_1T_1}$ do not support rISC between T_1 and S_1 to happen in gas phase. On the other hand, the difference in energy between S_1 and the second triplet state T_2 is found significantly smaller. The QE conformer of **PTZ-OMe** stands out with a T_2 computed at 0.42 eV above S_1. In all other cases, T_2 is predicted below S_1 in gas phase, with the largest $\Delta E_{S_1T_2}$ amounting to 0.29 eV for the QE conformer of **DMAC-T-Ph**. All dyes have at least one conformation for which $\Delta E_{S_1T_2}$ is almost vanishing. Computed spin-orbit couplings $SOCME_{S_1T_2}$ are found sizeable in most cases, between 0.40 cm^{-1} (QA of **DMAC-Ph**) and 2.19 cm^{-1} (QE of **DMAC-T-Ph**). Despite the clear limitations of a model based on wavefunction calculations conducted in gas phase, thus lacking conformational and dynamic disorder as well as the interaction with the solvation or polymer matrix environment,[43,44,52] the intrinsically small $\Delta E_{S_1T_2}$ along with the sizeable $SOCME_{S_1T_2}$ values suggest a more favorable rISC between the second triplet state and the first singlet excited state, except for **PTZ-OMe**. For PXZ substituted analogue described by Li *et al.*,[33] in contrast to our study, the computational results yielded a maximum of 0.22 eV, suggesting the possibility of rISC between the singlet S_1 and triplet T_1 states. However, due to the lack of SOCME calculations and triplet states orbitals, as well as a different level of theory, a direct comparison between both series is not feasible. The main distinction between the two studies is the emphasis placed on the potential involvement of both conformers in the photophysical properties, in addition to the presence of HLCT states, which favor both rISC and fluorescence.

Although the singlet-triplet splitting and SOCME values indicate that the transition may occur in the QA conformer such as for **DMAC-Ph** (as shown in Table 5), experimental measurements indicate that the delayed fluorescence is observed in PMMA. As X-ray diffraction hints, the QE conformation is favored in such a condensed phase. Experimentally, no measurements hint toward delayed fluorescence occurring in the QA conformation. This observation is consistent with previous studies who concluded that TADF happens predominantly in the QE conformer, where measurement consistently showed larger singlet-triplet splitting in the QA conformer preventing efficient rISC.[45–47]

The calculated results for **DMAC-OMe**, as presented in Table 5, indicate that this compound exhibits a low ΔE_{ST} value between S_1 and T_2, as well as a significant SOCME. However, this emitter does not exhibit any experimental delayed fluorescence, neither in solution nor in a PMMA matrix. As **DMAC-OMe** seems to deviate from the calculated trend, the observed differences can be attributed to various modelling approximations. The calculations were performed in the gas phase, thus not including a model for the solvent (implicit or explicit) or for the solid PMMA matrix. It is possible that a polar environment may impact the CT character of the molecules, affecting both the ΔE_{ST} and SOCME values. Furthermore, it can

Table 5. Calculated ΔE_{ST} between S_1 and T_1 ($\Delta E_{S_1T_1}$) and between S_1 and T_2 ($\Delta E_{S_1T_2}$), defined as the difference between the energies of their potential minima,[7] along with the corresponding Spin-Orbit Coupling Matrix Element (SOCME), computed at the respective optimized triplet geometries.

Compound	Conformation	$\Delta E_{S_1T_1}$ (eV)	$\Delta E_{S_1T_2}$ (eV)	$SOCME_{S_1T_1}$ (cm^{-1})	$SOCME_{S_1T_2}$ (cm^{-1})
DMAC-Ph	QE	0.69	0.07	1.52	0.54
	QA	0.66	0.02	0.42	0.40
DMAC-T-Ph	QE	0.89	0.29	0.78	2.19
	QA	0.58	0.01	0.83	0.48
PTZ-T-Ph	QE	0.62	0.22	0.51	1.42
	QA	0.60	0.01	0.81	0.47
DMAC-OMe	QE	0.56	0.01	0.40	1.35
PTZ-OMe	QE	0.50	−0.42	0.06	1.52
	QA	0.82	0.13	0.08	0.63
PXZ-OMe	QE	0.38	0.11	0.05	0.60

© 2024 The Author(s). ChemPhotoChem published by Wiley-VCH GmbH

be hypothesized that a photophysical pathway may exist where the rISC process is in competition with an ISC conversion due to the low ΔE_{ST}, thus preventing efficient rISC and favouring vibrational de-excitation towards the lower-lying triplet state.

Besides, qualitative trends of $SOCME_{S_1T_1}$ and $SOCME_{S_1T_2}$ values can be rationalized by comparing the nature of the singlet and triplet excited states. Here we proceed with the NTOs computed at the first singlet excited state considering that their geometries are close to that of the excited triplet state of interest. Figure 7 illustrates the NTOs computed at the QE and QA geometries of the first (T_1) and second (T_2) triplet states for a representative molecule (**DMAC-Ph**) (see Figures S42–S47 for the other compounds). For example, the QE conformer of **DMAC-Ph** exhibits a S_1 with a clear ^{1}n–π* character (Figure 6) whereas T_1 and T_2 present a ^{3}π–π* character, thus the transition from the triplet manifold to the singlet state involves a change of orbital type and the corresponding $SOCME_{S_1T_i}$ are sizeable. For the QA conformation, the $SOCME_{S_1T_i}$ are generally smaller because in most cases S_1, T_1 and T_2 have a π–π* character with similar NTOs.

Conclusions

In this study, we carefully investigated a series of push-pull fluorophores, focusing on their photophysical properties and potential for TADF. All six fluorophores were based on a quinazoline acceptor unit, along with either a phenyl or methoxy moiety, and a phenylene or thienylene linker. The electron-donating moiety consisted of a bulky 9,9-dimethylacridan, phenoxazine, or phenothiazine fragment. In solution, all dyes undergo short-lived fluorescence.

For four out of the six fluorophores, quantum chemical calculations suggested the possible presence of two conformers, namely QE and QA, which could be contributing to the structure of the emission UV/Vis spectra as well as delayed fluorescence. Notably, compared to the QE conformer, QA exhibited a more emissive character, characterized by larger oscillator strengths thanks to a π–π*/LE nature of the transition orbitals, significantly delocalized over the molecular backbone. For the other two dyes, **DMAC-OMe** and **PXZ-OMe**, the QE $S_1 \rightarrow S_0$ transition gains hybrid HLCT character, resulting in fair oscillator strength compatible with the observed prompt fluorescence.

Among the four molecules for which the QA conformer was evidenced in gas phase wave-function simulations, three of them, namely **DMAC-Ph**, **DMAC-T-Ph** and **PTZ-T-Ph**, stood out for their experimentally measured microsecond scale fluorescence lifetime in PMMA films, indicative of TADF behavior. Calculations predicted for the fourth, **PTZ-OMe**, an unlikely rISC for the QE conformer, whereas it is for QA. This is the main distinctive feature to correlate with the absence of experimentally observed delayed fluorescence in **PTZ-OMe**. On the other hand, both conformers of the phenyl-substituted quinazoline derivatives have triplet states with sufficient coupling between the S_1 and T_2 states (smallest for QA), along with low values of $\Delta E_{S_1T_2}$ (largest for QE), whereas $\Delta E_{S_1T_1}$ are larger than 0.2 eV. Thus, the first triplet state is not expected to participate directly in the rISC process that allows delayed fluorescence.

Noteworthy, TADF is found likely to occur in the solid state only for dyes with a predicted coexistence of QA and QE conformers, and with a rISC predicted to be efficient in this latter conformation. This is in line with the suggestion that in solid state the conformational relaxation of the QE conformer is hindered, and that coexistence of features specific to each conformer are key for TADF to happen.

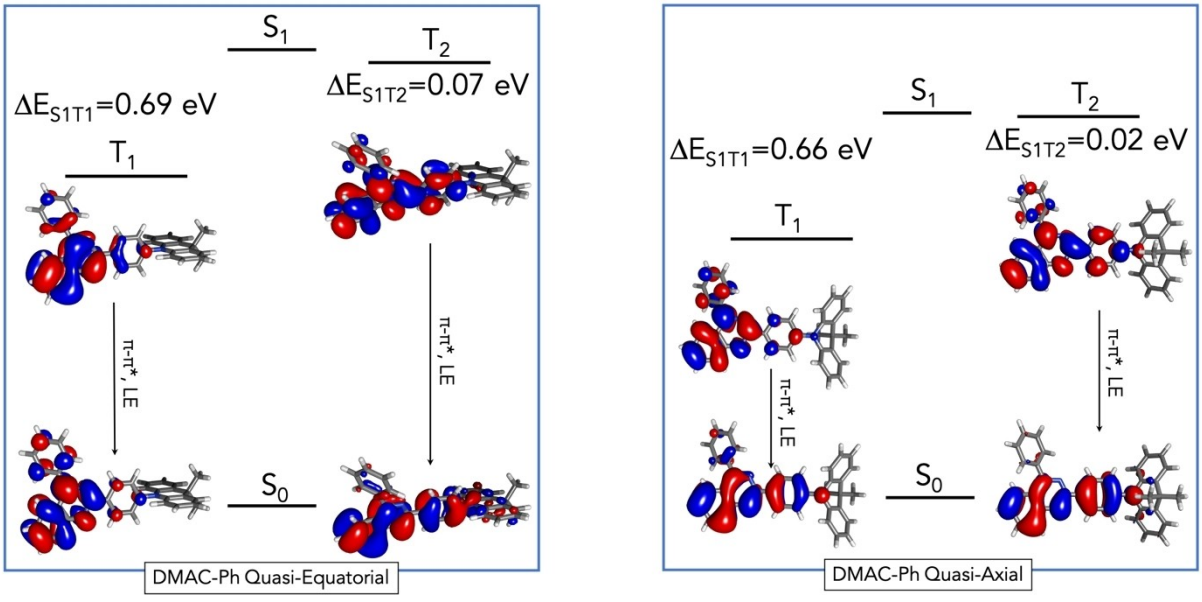

Figure 7. NTOs computed at the QE and QA geometries of the first (T_1) and second (T_2) triplet states of **DMAC-Ph** (isovalue of 0.02 e^-/au^3).

© 2024 The Author(s). ChemPhotoChem published by Wiley-VCH GmbH

23670932, 0, Downloaded from https://chemistry-europe.onlinelibrary.wiley.com/doi/10.1002/cptc.202400259 by Université De Rennes, Wiley Online Library on [13/11/2024]. See the Terms and Conditions (https://onlinelibrary.wiley.com/terms-and-conditions) on Wiley Online Library for rules of use; OA articles are governed by the applicable Creative Commons License

Experimental Details

Materials and Methods

All solvents were reagent grade for synthesis. Starting materials were purchased from Sigma-Aldrich or TCI and were used without further purification. Thin layer chromatography (TLC) was conducted on pre-coated aluminum sheets with 0.20 mm Merck Alugram SIL G/UV254 with fluorescent indicator UV254 and 0.25 mm Merck silica gel (60-F254). Column chromatography was carried out using Acros silica gel 60 (particle size 63–200 μm).

NMR spectra were recorded in $CDCl_3$ on a Bruker AC-300 spectrometer. The chemical shifts δ are reported in ppm and are referenced to the appropriate solvent signals of $CDCl_3$ (^1H, $\delta =$ 7.27 ppm; ^{13}C, $\delta = 77.0$ ppm). The coupling constants J are given in Hz. In the ^1H NMR spectra, the following abbreviations are used to describe the peak patterns: s (singlet), d (doublet), t (triplet), q (quadruplet), m (multiplet). Acidic impurities in $CDCl_3$ were removed by treatment with solid K_2CO_3. High-resolution mass analyses were carried out at the 'Centre Régional de Mesures Physiques de l'Ouest' (CRMPO, Université de Rennes 1) using a Bruker MicroTOF-Q II instrument.

Absorption spectra were recorded using a dual-beam grating Schimadzu UV-3000 absorption spectrometer with a quartz cell of 1 cm of optical path length. The steady-state fluorescence emission spectra were recorded by using a Horiba S2 Jobin Yvon Fluoromax 4 or a Spex Fluoromax-3 Jobin-Yvon Horiba spectrofluorometer. All fluorescence and excitation spectra were corrected to take into account the response of the photomultiplier. Fluorescence quantum yields (±10%) were determined relative to the indicated reference. PMMA films were prepared by mixing 1% wt (1 mg) of chromophore with PMMA (100 mg) in THF and by subsequent drop casting method.

General procedure for synthesis of intermediates 1 and 2. A mixture of 2-aminobenzophenone (0.394 g, 2 mmol), corresponding aromatic aldehyde (2 mmol), ammonium acetate (0.616 g, 8 mmol) and iodine (0.508 g, 2 mmol) in EtOH (20 mL) was stirred at room temperature for 19 or 24 h. After completion of the reaction, formed precipitate was filtered off and washed with water.

2-(4-Bromophenyl)-4-phenylquinazoline 1. Synthesis was accomplished following the general procedure. Reaction time was 19 h. Colorless solid, yield 76% (549 mg), mp: 180–182 °C (mp lit.:[53] 192–194 °C) ^1H NMR (300 MHz, $CDCl_3$): δ 7.54–7.67 (m, 6H), 7.86–7.93 (m, 3H), 8.13–8.16 (m, 2H), 8.57–8.60 (d, $^3J = 8.3$ Hz, 2H; C_6H_4Br).

2-(5-Bromothiophen-2-yl)-4-phenylquinazoline 2. Synthesis was accomplished following the general procedure. Reaction time was 24 h. Colorless solid, yield 69% (506 mg), mp: 158–160 °C. ^1H NMR (300 MHz, $CDCl_3$): δ 7.13 (d, $^3J = 3.8$ Hz, 1H; thioph.), 7.49–7.60 (m, 4H), 7.82–7.93 (m, 4H), 8.03–8.10 (m, 3H). ^{13}C NMR (75 MHz, $CDCl_3$): δ 117.4, 121.8, 127.1, 127.4, 128.7, 128.8, 129.3, 130.3, 131.4, 134.0, 137.3, 145.6, 151.9, 156.4, 168.7.

4-Methoxy-2-(4-bromophenyl)quinazoline 3. To a solution of 4-chloro-2-(4-bromophenyl) quinazoline (0.447 g, 1.4 mmol) in 2.8 mL of abs. CH_3OH a solution of CH_3ONa in CH_3OH (prepared from Na (0.032 g) and absolute CH_3OH (1 mL)) was added. The reaction mixture was refluxed for 3 h. After completion the solvent was evaporated. Water (10 mL) and EtOAc (10 mL) were added to the residue. The organic layer was separated and solvent was evaporated under vacuum. Colorless solid, yield 75% (335 mg), mp: 144–146 °C (mp: lit.:[54] 119 °C). ^1H NMR (300 MHz, $CDCl_3$): δ 4.28 (s, 1H, OCH_3), 7.52–7.55 (m, 1H; quinaz.), 7.62–7.65 (m, 2H; C_6H_4Br), 7.80–7.85 (m, 1H; quinaz.), 7.96–7.98 (m, 1H; quinaz.), 8.14–8.17 (m, 1H; quinaz.), 8.45–8.50 (m, 2H; C_6H_4Br).

General procedure I for by Buchwald-Hartwig cross-coupling reaction. $Pd(OAc)_2$ (31 mg, 0.14 mmol) and $P(tBu)_3HBF_4$ (49 mg, 0.17 mmol) were added to the mixture of bromoderivative **1** or **3** (0.70 mmol) acridine, phenothiazine or phenoxazine (1.40 mmol), K_2CO_3 (0.26 g, 1.89 mmol) in degassed toluene (5 mL). The resulting mixture was refluxed under nitrogen atmosphere for 3 days. The reaction mixture was cooled and EtOAc/water mixture (1:1, 10 mL) was added. The organic layer was separated and the aqueous layer was extracted with additional EtOAc (2×10 mL). The solvent was evaporated under reduced pressure and product was purified by column chromatography.

General procedure II for by Buchwald-Hartwig cross coupling reaction. Pd_2dba_3 (75 mg, 81.9 μmol) and $P(tBu)_3HBF_4$ (29 mg, 100 μmol) were added to the mixture of the bromoderivative (0.41 mmol), 9,10-dihydro-9,9-dimethylacridine, phenothiazine or phenoxazine (0.82 mmol), *t*BuONa (0.11 g, 1.1 mmol) in degassed toluene (3.5 mL). The resulting mixture was refluxed under nitrogen atmosphere for 3 days. The reaction mixture was cooled and EtOAc/water mixture (1:1, 10 mL) was added. The organic layer was separated and the aqueous layer was extracted with additional EtOAc (2×10 mL). The solvent was evaporated under reduced pressure and product was purified by column chromatography.

4-Phenyl-2-(4-(9,9-dimethyl-9,10-dihydroacridin-10-yl)phenyl)quinazoline DMAC-Ph. Synthesis was accomplished following the general procedure I. The product was purified by column chromatography (SiO_2, petroleum ether/EtOAc (19:1)) and washed with hexane. Pale yellow solid, yield 77% (264 mg), mp: 202–204 °C. ^1H NMR (300 MHz, $CDCl_3$): δ 1.72 (s, 6H; 2(CH_3)), 6.37–6.40 (m, 2H; acrid.), 6.93–6.98 (m, 4H; acrid.), 7.46–7.52 (m, 4H; acrid., phenylene), 7.61–7.64 (m, 4H; quinaz., Ph), 7.91–7.94 (m, 3H; quinaz., Ph), 8.17–8.19 (m, 2H; quinaz.), 8.90–8.93 (m, 2H; phenylene). ^{13}C NMR (75 MHz, $CDCl_3$): δ 31.5 (2(CH_3)), 36.2 ($C(CH_3)_2$), 114.3, 120.8, 121.9, 125.4, 126.5, 127.3, 127.5, 128.8, 129.4, 130.2, 130.3, 131.4, 136.6, 137.8, 138.4, 140.9, 143.5, 152.2, 159.9, 168.8. HRMS (ESI) *m/z* calcd for $C_{35}H_{28}N_3^+$ ($[M+H]^+$): 490.2277; found: 490.2275.

4-Phenyl-2-(5-(9,9-dimethyl-9,10-dihydroacridin-10-yl)thiophen-2-yl)quinazoline DMAC-T-Ph. Synthesis was accomplished following the general procedure II. The product was purified by column chromatography (SiO_2, petroleum ether/EtOAc (9:1)) and washed with heptane. Yellow solid, yield 66% (134 mg), mp: 230–232 °C. ^1H NMR (300 MHz, $CDCl_3$): δ 1.69 (s, 6H; 2(CH_3)), 6.83–6.87 (m, 2H; acrid.), 6.97–7.13 (m, 5H; acrid., thiophen.), 7.45–7.48 (m, 2H; acrid.), 7.54–7.60 (m, 4H; quinaz., Ph), 7.86–7.88 (m, 3H; quinaz., Ph), 8.07–8.14 (m, 2H; quinaz.), 8.28 (d, $^3J = 3.9$ Hz, 1H; thiophen.). ^{13}C NMR (75 MHz, $CDCl_3$): δ 31.3 (2(CH_3)), 36.1 ($C(CH_3)_2$), 115.2, 121.8, 125.2, 126.8, 128.7, 129.0, 130.3, 130.4, 131.3, 134.0, 137.4, 141.0, 143.5, 147.3, 152.0, 156.9, 168.7. HRMS (ESI) *m/z* calcd for $C_{33}H_{26}N_3S^+$ ($[M+H]^+$): 496.1842 ; found: 496.1845

4-Phenyl-2-(5-(10*H*-phenothiazin-10-yl)thiophen-2-yl)quinazoline PTZ-T-Ph. Synthesis was accomplished following the general procedure II. The product was purified by column chromatography (Al_2O_3, petroleum ether/EtOAc (9:1)) and recrystallization from CH_2Cl_2/heptane mixture. Bright yellow solid, yield 53% (106 mg), mp: 139–141 °C. ^1H NMR (300 MHz, $CDCl_3$): δ 6.91–6.97 (m, 4H; phenothiaz.), 7.00–7.06 (m, 3H; thioph., phenothiaz.), 7.10–7.12 (m, 2H; phenothiaz.), 7.50–7.55 (m, 1H; quinaz.), 7.84–7.89 (m, 3H; Ph), 8.04–8.11 (m, 2H; quinaz., Ph), 8.18 (d, $^3J = 3.9$ Hz, 1H; thiophen.). ^{13}C NMR (75 MHz, $CDCl_3$): δ 118.4, 121.7, 123.3, 123.9, 126.5, 127.0, 127.1, 127.3, 127.4, 128.7, 128.8, 128.9, 130.2, 130.3, 134.0, 137.4, 141.3, 143.8, 148.8, 152.0, 156.9, 168.6. HRMS (ESI) *m/z* calcd for $C_{30}H_{20}N_3S_2^+$ $[M+H]^+$: 486.1093; found: 486,1092.

© 2024 The Author(s). ChemPhotoChem published by Wiley-VCH GmbH

23670932, 0, Downloaded from https://chemistry-europe.onlinelibrary.wiley.com/doi/10.1002/cptc.202400259 by Université De Rennes, Wiley Online Library on [13/11/2024]. See the Terms and Conditions (https://onlinelibrary.wiley.com/terms-and-conditions) on Wiley Online Library for rules of use; OA articles are governed by the applicable Creative Commons License

4-Methoxy-2-(4-(9,9-dimethyl-9,10-dihydroacridin-10-yl)phenyl)quinazoline DMAC-OMe. Synthesis was accomplished following the general procedure I. The product was purified by column chromatography (Al_2O_3, petroleum ether/EtOAc (19:1)). Pale yellow solid, yield 92% (286 mg), mp: 211–213 °C. ^{1}H NMR (300 MHz, $CDCl_3$): δ 1.72 (s, 6H; 2(CH_3)), 4.34 (s, 3H; OCH_3), 6.37–6.40 (m, 2H; acrid.), 6.91–7.00 (m, 4H; acrid.), 7.46–7.50 (m, 4H; acrid., phenylene), 7.54–7.59 (m, 1H; quinaz.), 7.84–7.89 (m, 1H; quinaz.), 8.02–8.05 (m, 1H; quinaz.), 8.20–8.23 (m, 1H; quinaz.), 8.84 (d, ^3J= 8.4 Hz, 2H; phenylene). ^{13}C NMR (75 MHz, $CDCl_3$): δ 31.5 (2(CH_3)), 36.2 ($C(CH_3)_2$), 54.4 (OCH_3), 114.3, 115.5, 120.8, 123.7, 125.4, 126.5, 126.9, 128.2, 130.2, 131.2, 131.5, 133.8, 138.3, 140.9, 143.5, 152.0, 159.6, 167.5. HRMS (ESI) *m/z* calcd for $C_{30}H_{26}N_3O^+$ $[M+H]^+$: 444.2070; found: 444.2077.

4-Methoxy-2-(4-(10*H*-phenothiazin-10-yl)phenyl)quinazoline PTZ-OMe. Synthesis was accomplished following the general procedure I. The product was purified by column chromatography (Al_2O_3, petroleum ether/EtOAc (19:1)). Pale yellow solid, yield 39% (118 mg), mp: 188–190 °C. ^{1}H NMR (300 MHz, $CDCl_3$): δ 4.32 (s, 3H; OCH_3), 6.39–6.42 (m, 2H; phenothiaz.), 6.85–6.90 (m, 4H; phenothiaz.), 7.06–7.09 (m, 2H; phenothiaz.), 7.50–7.58 (m, 3H; phenylene, quinaz.), 7.85–7.88 (m, 1H; quinaz.), 8.00–8.03 (m, 1H; quinaz.), 8.18–8.21 (m, 1H; quinaz.), 8.78 (d, ^3J=8.6 Hz, 2H; phenylene). ^{13}C NMR (75 MHz, $CDCl_3$): δ 54.3 (OCH_3), 115.5, 117.2, 121.5, 123.0, 123.7, 126.8, 127.1, 128.2, 129.7, 131.0, 133.8, 137.7, 143.6, 144.1, 152.0, 159.5, 167.4. HRMS (ESI) *m/z* calcd for $C_{27}H_{20}N_3OS^+$ $[M+H]^+$: 434.1322; found: 434.1320.

4-Methoxy-2-(4-(10*H*-phenoxazin-10-yl)phenyl)quinazoline PXZ-OMe. Synthesis was accomplished following the general procedure I. The product was purified by column chromatography (Al_2O_3, petroleum ether/EtOAc (19:1)). Yellow solid, yield 91% (266 mg), mp: 198–200 °C. ^{1}H NMR (300 MHz, $CDCl_3$): δ 4.33 (s, 3H; OCH_3), 6.02–6.05 (m, 2H; phenoxaz.), 6.57–6.73 (m, 6H; phenoxaz.), 7.48–7.59 (m, 3H; phenylene, quinaz.), 7.86–7.89 (m, 1H; quinaz.), 8.01–8.03 (m, 1H; quinaz.), 8.21–8.22 (m, 1H; quinaz.), 8.80 (d, ^3J=8.4 Hz, 2H; phenylene). ^{13}C NMR (75 MHz, $CDCl_3$): δ 54.4 (OCH_3), 113.5, 115.5, 115.6, 121.5, 123.4, 123.7, 126.9, 128.2, 131.0, 131.3, 133.8, 134.4, 138.6, 141.1, 144.1, 152.0, 159.4, 167.5. HRMS (ESI) *m/z* calcd for $C_{27}H_{20}N_3O_2^+$ $[M+H]^+$: 418.1550; found: 418.1553.

Computational Details

Theoretical investigations conducted in this work rely on wave-function based methodologies, namely the Approximate Singles and Doubles Coupled Cluster (CC2) of theory.[55,56] Such methods have recently been proven accurate for the estimation of the ΔE_{ST} value and the characterization of the electronic states relevant to the rISC,[6,10] as they allow to avoid the functional-dependency of Density Functional (DFT) based models. Meanwhile, being computationally more demanding, calculations are limited to gas phase. Ground and excited singlet as well as triplet state geometries, electronic energies, transition properties (transition energies, oscillator strengths, NTOs) were computed at the CC2 level of theory in gas phase. The triple zeta def2-TZVP basis set was used, along with the Spin-Component Scaling (SCS) approximation.[57] CC2 calculations were conducted using the Turbomole 7.5.1 package.[58] SOCME calculations were obtained at the TD-DFT M06-2X/TZVP level of theory, using CC2 T_1 and T_2 geometries in the gas phase, with the ADF 2020 code.[59]

X-ray Structure

Deposition Number https://www.ccdc.cam.ac.uk/services/structures?id=doi:10.1002/cptc.202400259" 2339313 (for **PTZ-OMe**), contains the supplementary crystallographic data for this paper. These data are provided free of charge by the joint Cambridge Crystallographic Data Centre and Fachinformationszentrum Karlsruhe http://www.ccdc.cam.ac.uk/structures Access Structures service.

Acknowledgements

SA, AF, CK and MH are grateful to the EUR LUMOMAT project and the Investments for the Future program ANR-18-EURE-0012. TNM thanks the French Ambassy in Moscow for a mobility grant in 2021 (Ostrogradski Program) and the Ministry of Science and Higher Education of the Russian Federation (Ural Federal University Program of Development within the Priority-2030 Program). SA acknowledges the Junta de Comunidades de Castilla-La Mancha/FEDER (project SBPLY/21/180501/000042).

Conflict of Interests

The authors declare no conflict of interest.

Data Availability Statement

The data that support the findings of this study are available from the corresponding author upon reasonable request.

Keywords: Computational Chemistry · Dyes · Heterocycles · Quinazoline · Thermally-activated Delayed Fluorescence

[1] Z. Yang, Z. Mao, Z. Xie, Y. Zhang, S. Liu, J. Zhao, J. Xu, Z. Chi, M. P. Aldred, *Chem. Soc. Rev.* **2017**, *46*, 915–1016.
[2] C. Adachi, M. A. Baldo, M. E. Thompson, S. R. Forrest, *J. Appl. Phys.* **2001**, *90*, 5048–5051.
[3] Y. Tao, K. Yuan, T. Chen, P. Xu, H. Li, R. Chen, C. Zheng, L. Zhang, W. Huang, *Adv. Mater.* **2014**, *26*, 7931–7958.
[4] M. Y. Wong, E. Zysman-Colman, *Adv. Mater.* **2017**, *29*, 1605444.
[5] F. B. Dias, K. N. Bourdakos, V. Jankus, K. C. Moss, K. T. Kamtekar, V. Bhalla, J. Santos, M. R. Bryce, A. P. Monkman, *Adv. Mater.* **2013**, *25*, 3707–3714.
[6] D. Hall, S. M. Suresh, P. L. dos Santos, E. Duda, S. Bagnich, A. Pershin, P. Rajamalli, D. B. Cordes, A. M. Z. Slawin, D. Beljonne, A. Köhler, I. D. W. Samuel, Y. Olivier, E. Zysman-Colman, *Adv. Opt. Mater.* **2020**, *8*, 1901627.
[7] P. K. Samanta, D. Kim, V. Coropceanu, J.-L. Brédas, *J. Am. Chem. Soc.* **2017**, *139*, 4042–4051.
[8] C. M. Marian, *Annu. Rev. Phys. Chem.* **2021**, *72*, 617–640.
[9] C. M. Marian, *Wiley Interdiscip. Rev. Comput. Mol. Sci.* **2012**, *2*, 187–203.
[10] A. Pershin, D. Hall, V. Lemaur, J.-C. Sancho-Garcia, L. Muccioli, E. Zysman-Colman, D. Beljonne, Y. Olivier, *Nat. Commun.* **2019**, *10*, 597.
[11] R. Dhali, D. K. A. Phan Huu, F. Bertocchi, C. Sissa, F. Terenziani, A. Painelli, *Phys. Chem. Chem. Phys.* **2021**, *3*, 378–387.
[12] M. A. El-Sayed, *Acc. Chem. Res.* **1968**, *1*, 8–16.
[13] T. J. Penfold, E. Gindensperger, C. Daniel, C. M. Marian, *Chem. Rev.* **2018**, *118*, 6975–7025.
[14] M. K. Etherington, J. Gibson, H. F. Higginbotham, T. J. Penfold, A. P. Monkman, *Nat. Commun.* **2016**, *7*, 13680.
[15] F. B. Dias, J. Santos, D. R. Graves, P. Data, R. S. Nobuyasu, M. A. Fox, A. S. Batsanov, T. Palmeira, M. N. Berberan-Santos, M. R. Bryce, A. P. Monkman, *Adv. Sci.* **2016**, *3*, 1600080.
[16] X.-K. Chen, D. Kim, J.-L. Brédas, *Acc. Chem. Res.* **2018**, *51*, 2215–2224.
[17] W. Li, Y. Pan, R. Xiao, Q. Peng, S. Zhang, D. Ma, F. Li, F. Shen, Y. Wang, B. Yang, Y. Ma, *Adv. Funct. Mater.* **2014**, *24*, 1609–1614.

© 2024 The Author(s). ChemPhotoChem published by Wiley-VCH GmbH

23670932, 0, Downloaded from https://chemistry-europe.onlinelibrary.wiley.com/doi/10.1002/cptc.202400259 by Université De Rennes, Wiley Online Library on [13/11/2024]. See the Terms and Conditions (https://onlinelibrary.wiley.com/terms-and-conditions) on Wiley Online Library for rules of use; OA articles are governed by the applicable Creative Commons License

[18] J. Li, M. Zhang, T. Li, D. Guo, T. Tian, H. Zhang, *J. Mater. Chem. C* **2022**, *10*, 13124–13136.
[19] J. M. Jacob, P. K. Samanta, M. K. Ravva, *New J. Chem.* **2023**, *47*, 10552–10563.
[20] X. Wang, G. Zhao, T. Gao, G. Zhang, H. Chen, T. Zhou, Z. Zhang, W. Tian, W. Jiang, Y. Sun, *J. Mater. Chem. C* **2024**, *12*, 5019–5027.
[21] J. Wiefermann, J. M. M. Kaminski, E. Pankert, D. Hertel, K. Meerholz, C. M. M. Marian, T. J. J. Mueller, *ChemPhotoChem* **2023**, *7*, e202200265.
[22] G. N. Lipunova, E. V. Nosova, V. N. Charushin, O. N. Chupakhin, *Curr. Org. Synth.* **2018**, *15*, 793–814.
[23] E. V. Nosova, S. Achelle, G. N. Lipunova, V. N. Charushin, O. N. Chupakhin, *Russ. Chem. Rev.* **2019**, *88*, 1128–1178.
[24] T. N. Moshkina, P. le Poul, A. Barsella, O. Pytela, F. Bureš, F. Robin-le Guen, S. Achelle, E. V. Nosova, G. N. Lipunova, V. N. Charushin, *Eur. J. Org. Chem.* **2020**, *33*, 5445–5454.
[25] A. E. Kopotilova, M. I. Valieva, E. S. Starnovskaya, T. N. Moshkina, E. V. Nosova, O. S. Taniya, A. A. Kalinichev, D. S. Kopchuk, P. A. Slepukhin, V. S. Goviko, G. A. Kim, V. N. Charushin, *J. Photochem. Photobiol. A* **2024**, *448*, 115350.
[26] R. Plaza-Pedroche, D. Georgiou, M. Fakis, A. Fihey, C. Katan, F. Robin-le Guen, S. Achelle, J. Rodríguez-López, *Dyes Pigm.* **2021**, *185*, 108948.
[27] S. Achelle, J. Rodríguez-López, F. Robin-le Guen, *J. Org. Chem.* **2014**, *79*, 7564–7571.
[28] D. Liu, Z. Zhang, H. Zhang, Y. Wang, *Chem. Commun.* **2013**, *49*, 10001–10003.
[29] B. Li, Z. Wong, S.-J. Su, F. Guo, Y. Cao, Y. Zhang, *Adv. Opt. Mater.* **2019**, *7*, 1801496.
[30] B. Li, Z. Li, F. Guo, J. Song, X. Jiang, Y. Wang, S. Gao, J. Wang, X. Pang, L. Zhao, Y. Zhang, *ACS Appl. Mater. Interfaces* **2020**, *12*, 14233–14243.
[31] P. Li, Y. Xiang, S. Gong, W.-K. Lee, Y.-H. Huang, C.-Y. Wang, C. Yang, C.-C. Wu, *J. Mater. Chem. C* **2021**, *9*, 12633–12641.
[32] X. Song, S. Shen, S. Zou, Y. Wang, F. Guo, S. Gao, Y. Zhang, *Chem. Eng. J.* **2014**, *481*, 148794.
[33] B. Li, Z. Wang, S.-J. Su, F. Guo, Y. Gao, Y. Zhang, *Adv. Opt. Mater.* **2019**, *7*, 1801496.
[34] B. Li, Z. Li, Q. Xia, X. Song, D. Chen, F. Guo, S. Gao, Y. Wang, Y. Zhang, *J. Mater. Chem. C* **2022**, *10*, 16064–16069.
[35] S. K. Panja, N. Dwivedi, S. Saha, *Tetrahedron Lett.* **2012**, *53*, 6167–6172.
[36] S. G. Baram, O. P. Shkurko, V. P. Mamaev, *Bull. Acad. Sci. USSR, Div. Chem. Sci.* **1991**, *40*, 601–605.
[37] T. N. Moshkina, E. V. Nosova, J. V. Permyakova, G. N. Lipunova, M. S. Valova, P. A. Slepukhin, L. K. Sadieva, V. N. Charushin, *Dyes Pigm.* **2022**, *206*, 110592.
[38] M. Hodée, J. Massue, S. Achelle, A. Fihey, D. Tondelier, G. Ulrich, F. Robin-le Guen, C. Katan, *Phys. Chem. Chem. Phys.* **2023**, *25*, 32699–32708.
[39] J. Massue, L. Diarra, I. Georgoulis, A. Fihey, F. Robin-le Guen, G. Ulrich, M. Fakis, S. Achelle, *ChemPhotoChem* **2023**, *7*, e202300085.
[40] F. K. Merkt, T. J. J. Müller, *Sci. China Chem.* **2018**, *61*, 909–924.
[41] A. C. Jahnke, M. Spulber, M. Neuburger, C. G. Palivan, O. S. Wenger, *Chem. Commun.* **2014**, *50*, 10883–10886.
[42] Z.-Y. Xing, Q. Zhao, Y. Fu, F. Ye, *Chem. Heterocycl. Compd.* **2011**, *47*, 607–610.
[43] T. J. Penfold, F. B. Dias, A. P. Monkman, *Chem. Commun.* **2018**, *54*, 3926–3935.
[44] K. Stavrou, L. G. Franca, T. Böhmer, L. M. Duben, C. M. Marian, A. P. Monkman, *Adv. Funct. Mater.* **2023**, *33*, 2300910.
[45] H. Tanaka, K. Shizu, H. Nakanotani, C. Adachi, *J. Phys. Chem. C* **2014**, *118*, 15985–15994.
[46] T. Serevičius, R. Skaigiris, J. Dodonova, L. Jagintavičius, J. Bucevičius, K. Kazlauskas, S. Juršėnas, S. Tumkevičius, *Chem. Commun.* **2019**, *55*, 1975–1978.
[47] T. Ryu, K. Miyata, M. Saigo, Y. Shimoda, Y. Tsuchiya, H. Nakanotani, C. Adachi, K. Onda, *Chem. Phys. Lett.* **2022**, *809*, 140155.
[48] R. L. Martin, *J. Chem. Phys.* **2003**, *118*, 4775–4777.
[49] A. F. Buene, D. M. Almenningen, *J. Mater. Chem. C* **2021**, *9*, 11974–11994.
[50] T. Miyamae, M. Haraguchi, Y. Tachi, S. Suzuki, M. Kozaki, K. Okada, *Org. Lett.* **2020**, *22*, 6790–6793.
[51] M. Etinski, C. M. Marian, *Phys. Chem. Chem. Phys.* **2017**, *19*, 13828–13837.
[52] F. Di Maiolo, D. K. A. Phun Huu, D. Giavazzi, A. Landi, O. Racchi, A. Painelli, *Chem. Sci.* **2024**, *15*, 3434–5450.
[53] Y. Yan, M. Shi, B. Niu, X. Meng, C. Zhu, G. Liu, T. Chen, Y. Liu, *RSC Adv.* **2016**, *6*, 36192–36197.
[54] L. Legrand, N. Lozac'h, *Bull. Soc. Chim. Fr.* **1963**, 1161–1166.
[55] C. Hättig, F. Weigend, *J. Chem. Phys.* **2000**, *113*, 5154.
[56] O. Christiansen, H. Koch, P. Jorgensen, *Chem. Phys. Lett.* **1995**, *243*, 409–418.
[57] A. Hellweg, S. A. Grün, C. Hättig, *Phys. Chem. Chem. Phys.* **2008**, *10*, 4119.
[58] S. G. Balasubramani, G. P. Chen, S. Coriani, M. Diedenhofen, M. S. Frank, Y. J. Franzke, F. Furche, R. Grotjahn, M. E. Harding, C. Hättig, A. Hellweg, B. Helmich-Paris, C. Holzer, U. Huniar, M. Kaupp, A. Marefat Khah, S. Karbalaei Khani, T. Müller, F. Mack, B. D. Nguyen, S. M. Parker, E. Perlt, D. Rappoport, K. Reiter, S. Roy, M. Rückert, G. Schmitz, M. Sierka, E. Tapavicza, D. P. Tew, C. van Wüllen, V. K. Voora, F. Weigend, A. Wodyński, J. M. Yu, *J. Chem. Phys.* **2020**, *152*, 184107.
[59] G. te Velde, F. M. Bickelhaupt, E. J. Baerends, C. Fonseca Guerra, S. J. A. van Gisbergen, J. G. Snijders, T. Ziegler, *J. Comput. Chem.* **2001**, *22*, 931–967.
[60] T. Nakagawa, S.-Y. Ku, K.-T. Wong, C. Adachi, *Chem. Commun.* **2012**, *48*, 9580–9582.
[61] Y. Tsuchiya, S. Diesing, F. Bencheikh, Y. Wada, P. L. dos Santos, H. Kaji, E. Zysman-Colman, I. D. W. Samuel, C. Adachi, *J. Phys. Chem. A* **2021**, *125*, 8074–8089.

Manuscript received: August 11, 2024
Revised manuscript received: October 1, 2024
Accepted manuscript online: October 1, 2024
Version of record online: ■■, ■■

© 2024 The Author(s). ChemPhotoChem published by Wiley-VCH GmbH

23670932, 0, Downloaded from https://chemistry-europe.onlinelibrary.wiley.com/doi/10.1002/cptc.202400259 by Université De Rennes, Wiley Online Library on [13/11/2024]. See the Terms and Conditions (https://onlinelibrary.wiley.com/terms-and-conditions) on Wiley Online Library for rules of use; OA articles are governed by the applicable Creative Commons License

RESEARCH ARTICLE

The prompt and thermally activated delayed fluorescence properties of a series of quinazoline chromophores were studied theoretically and experimentally. The effect of various structural modifications (phenyl or methoxy moiety on quinazoline core, phenylene or thienylene linker, dimethylacridan, phenoxazine or phenothiazine electron-donating groups) was thoroughly studied.

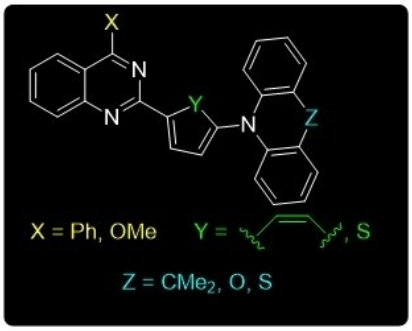

M. Hodée, T. N. Moshkina, J. Massue, A. Fihey*, T. Roisnel, C. Katan, E. Nosova, S. Achelle**

23670932, 0, Downloaded from https://chemistry-europe.onlinelibrary.wiley.com/doi/10.1002/cptc.202400259 by Université De Rennes, Wiley Online Library on [13/11/2024]. See the Terms and Conditions (https://onlinelibrary.wiley.com/terms-and-conditions) on Wiley Online Library for rules of use; OA articles are governed by the applicable Creative Commons License